Pieces of a puzzle: solar-wind power synergies on seasonal and diurnal timescales tend to be excellent worldwide

Nyenah, Emmanuel; Sterl, Sebastian; Thiery, Wim

Published in:
Environmental Research Communications

DOI:
10.1088/2515-7620/ac71fb

Publication date:
2022

ENVIRONMENTAL RESEARCH
COMMUNICATIONS

PAPER • OPEN ACCESS

Pieces of a puzzle: solar-wind power synergies on seasonal and diurnal timescales tend to be excellent worldwide

To cite this article: Emmanuel Nyenah *et al* 2022 *Environ. Res. Commun.* **4** 055011

Environmental Research Communications

PAPER

Pieces of a puzzle: solar-wind power synergies on seasonal and diurnal timescales tend to be excellent worldwide

Emmanuel Nyenah[1,*], **Sebastian Sterl**[1,2,3] and **Wim Thiery**[1]

[1] Vrije Universiteit Brussel, Department of Hydrology and Hydraulic Engineering, Brussels, Belgium
[2] KU Leuven, Department of Earth and Environmental Sciences, Leuven, Belgium
[3] International Renewable Energy Agency (IRENA), Bonn, Germany
[*] Author to whom any correspondence should be addressed.

E-mail: emmanuel.nyenah@vub.be **and** soineade@gmail.com

Keywords: solar-wind synergy, capacity factor, renewable electricity, hybrid output, open-access software, European copernicus cloud

Supplementary material for this article is available online

OPEN ACCESS

RECEIVED
25 February 2022

REVISED
9 May 2022

ACCEPTED FOR PUBLICATION
20 May 2022

PUBLISHED
31 May 2022

Abstract

Moving from fossil fuel-based electricity generation to renewable electricity generation is at the heart of current developments in power sectors worldwide. In this context, synergy assessment between renewable electricity sources is of great significance for local and regional power planning. Here we use synergy metrics (stability coefficient (C_{stab}) and normalised Pearson correlation coefficient (r) to a state-of-the-art reanalysis product from 2011–2020 to preliminarily assess solar-wind synergies globally on diurnal and seasonal time scales assuming equal installed capacities of solar and wind hybrid system. Our results suggest that medium-to-good diurnal and seasonal complementarities between solar photovoltaic and wind power potential are the norm, rather than the exception, which could help many countries in achieving balanced power mixes based on renewable resources. Our results also suggest that many regions in the tropics and sub tropics may need to explore synergic benefits of other renewables in addition to solar power. An open-access application is now available on the European Copernicus cloud to explore solar and wind synergies on diurnal and seasonal time scales worldwide.

1. Introduction

A global transition from fossil fuel-based energy to renewable energies could enable drastic reductions of CO_2 emissions, which is necessary to limit global warming to well below 2 °C, preferably to 1.5 °C, as decided in the Paris Agreement [1]. In this context, meeting electricity demand while supporting climate change mitigation is a central challenge for power sectors, which constitute an important component of the global energy sector.

Due to the cost-competitive and environment-friendly nature of renewable electricity (RE) [2–5], specifically from solar photovoltaic (PV) and wind power, RE has gained substantial attention as an alternative to fossil fuel-based power generation and supply to electricity grids around the world [6]. According to the 2021 annual report on renewable capacity statistics by the International Renewable Energy Agency (IRENA), more than 80% of all new electricity capacity added in 2020 was for renewable power generation, with solar PV and wind power plants accounting for 91% of this added RE capacity [7].

However, the variable and uncertain nature of wind and solar resources makes it difficult to design and operate a highly reliable electricity system that is majorly dependent on these renewable resources [5, 8, 9]. This variability leads to mismatches between supply and demand of electricity, which calls for electricity storage and hence require additional investments. According to literature, one potential solution to reduce storage needs is the hybridization of different RE sources [4], such as solar-wind hybridization, since mixes of RE sources may manifest a lower variability or be better aligned with demand than the individual RE sources constituting the mix [3, 10]. This has led to the concept of RE complementarity or synergy, which entails RE sources partially balancing each other [4, 11–13]. RE synergy can impact power systems by reducing electricity supply variability,

providing a supply and demand power balance, and thus potentially helping in lowering system cost (by reducing the dependence on storage) [3–5, 10, 14–19].

Synergy may exist both in the time domain (temporal complementarity) and in the space domain (spatial complementarity). A comprehensive assessment of solar-wind synergies thus requires a focus on various aspects of spatiotemporal complementarity [4]. In this work, we concentrate on spatiotemporal synergies between solar PV and wind power across all global land and covering both diurnal (hour-to-hour) and seasonal (month-to-month) synergies.

To quantify solar and wind synergy, various studies use statistical measures such as (anti)correlation-based [4, 10, 20–22] or variability-based [3, 10, 17, 18] metrics between the solar and wind power profiles. A recent study [3] showed that when such metrics are applied on hourly timescales, they typically fail to put realistic constraints on capacity factors of the considered resources. For example, if wind power potential cycle balances solar PV potential cycle–thus more wind at night than during the day—but the wind is weak, the diurnal (anti) correlation coefficients scores high for such complementarity, but one would need to increase the installed capacities of wind turbines to unrealistic levels to generate relevant power for balancing. This constraint led to the development of a new metric, the stability coefficient, which is a measure of the added value of wind power to balance daily electric power production from solar PV. This metric was used to assess hourly synergies of solar PV and wind power potential in West Africa using climate data from the state-of-the-art ERA5 reanalysis. The results obtained from this research showed that, if deployed smartly alongside solar PV, wind power could play a more important role in hybrid power systems in West Africa than maps of average wind resource strength would suggest, thanks to mutual resource complementarity on day-night scales.

On seasonal time scales, a widely used (anti)-correlation metric, the Pearson correlation coefficient, has been employed in several studies to assess spatiotemporal synergies between solar PV and wind, as found e.g. in the review of [4]. However, case studies on the assessment of spatiotemporal complementarity between solar and wind using the Pearson correlation tend to be highly region-specific. In addition, most literature has concentrated on Northern America, Brazil, Europe, West Africa, Australia, and China [4]. This spatial bias leaves large regions in Latin America, Africa, and Asia uncharted.

In this study, we aim to provide a comprehensive overview of solar-wind complementarity across a range of assumptions by extending previous regional spatiotemporal synergy analyses on hourly and monthly timescales between solar PV and wind power to the entire world (land only) using the stability coefficient and Pearson correlation coefficient respectively. We deliberately focus on land and assume that offshore solar PV power plays a negligible role in the energy transition. Understanding temporal and spatial distributions of renewable synergies on a global scale will not only be valuable in terms of communicating patterns and indicating the strength of local and regional synergies but may also play an important role in preliminary local and regional power planning and policy formulation. More specifically, we aim at answering the following research questions:

1. What is the global distribution of diurnal and seasonal synergy assuming equal installed capacities of solar PV and wind turbines (capacity ratio of 1:1)?
2. Is diurnal and seasonal solar-wind synergy in regions with reasonable solar and wind resource strength the norm or exception?

We also make use of the new European Copernicus cloud, the Climate Data Store (CDS) [23], to create an open-access software to investigate spatiotemporal solar PV and wind synergy.

The rest of the paper is organised as follows: section 2 focuses on the data and methodological framework used in the assessment of solar-wind synergy, section 3 presents major findings and discuss them in the light of available literature and section 4 presents the conclusion of the analysis.

2. Method

2.1. Analysis framework and RELITE software

Figure 1 summarises the framework used for synergy analysis and forms the framework for developing the synergy software (**R**enewable **El**ectric**i**ty Syn**e**rgy (*RELITE*)). The framework consists of three levels. In the first level, ERA5 fields are imported from the European Climate Data store and subsequently converted into capacity factors (second level). Third level involves power mixes and synergy analysis using stability coefficient (C_{stab}) and normalised Pearson correlation coefficient (r)) for diurnal and seasonal synergy analysis respectively. Here Installed capacity of solar and wind power are mixed according to any desired ratio (n:m). This study assumes a 1:1 capacity ratio. Setting this installed capacity ratio is specifically required for stability coefficient estimation. Hereafter, each of the three steps are described in detail.

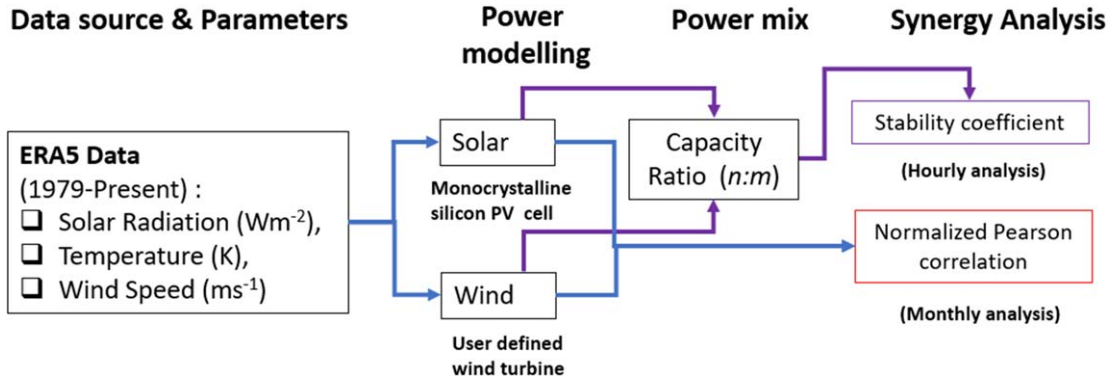

Figure 1. Schematic diagram for assessment framework and software development.

2.1.1. ERA5 data

Many studies report on the high quality of ERA5 data compared to direct measurements, which has led to its widespread use in energy and power modelling [3, 24–28].

To enable the estimation of solar photovoltaic and wind capacity factor, the following ERA5 data [28] are retrieved at hourly temporal resolution and at a spatial resolution of 0.25° from Climate Data Store:

1. Solar surface shortwave radiation downwards (ssrd) which correspond to Global Horizontal Irradiation, G, ($W\,m^{-2}$)
2. 2-m temperature (K).
3. Wind speed, V (ms^{-1}), at a hub height of 117 m is estimated from the atmospheric ERA-5 zonal (u) and meridional (v) wind speeds at 100 m and 10 m. The equation for estimating wind speed at the desired hub height can be found in [3].

Due to computational constraint for individual users on the Copernicus cloud, all meteorological fields are aggregated spatially to a 3° resolution and the time period is limited to 2011–2020 for global-scale (land-only) analysis presented in this study. In spite of the limited spatial resolution and temporal extent, results from this assessment are of importance for a large-scale assessment for solar wind complementarity. Moreover, users of our cloud-based software can easily perform similar analyses at higher spatial resolution and longer time periods over selected regions (including offshore ones).

2.1.2. Calculation of capacity factor (CF)

Capacity factors for two renewable technologies are calculated in this study: monocrystalline silicon-based solar PV cells and Vestas V126-3.3 wind turbines. For wind CF, the software allows for any wind turbine (with unique cut-in, nominal and cut-out wind speeds) to be used. The solar CF calculation is currently limited to monocrystalline silicon cells considering a fixed, flat mounting of solar panels.

2.1.2.1. Solar PV cells

Solar cell efficiency, η_{cell}, is modelled as a function of Global Horizontal Irradiation, denoted G, and ambient air temperature T, as shown by the equation (1) [3, 29]. We recognize that this selected approach is quite simplistic and while system-specific improvements are possible, they are unlikely to have a major impact on the outcomes and findings.

$$\eta_{cell}(G,\ T) = \eta_{ref}[1 - \beta(T_{cell}(G,\ T) - T_{ref}) + \gamma \log 10(G)] \quad (1)$$

where η_{ref} is the reference efficiency and coefficients β and γ reflect the cell material and structure. The characteristic value $\beta = 0.0045$ and $\gamma = 0.1$ for monocrystalline silicon cells are used [3, 29]. The reference temperature T_{ref} is 25 °C, and the cell temperature T_{cell} is calculated as a function of G and T by equation (2).

$$T_{cell}(G,\ T) = c_1 + c_2 T + c_3 G \quad (2)$$

where, the constants c_{1-3} also depend on cell properties. Values for c_{1-3} used are taken from [30] with $c_1 = -3.75\,°C, c_2 = 1.14, c_3 = 0.0175\,°C\,m^2\,W^{-1}$.

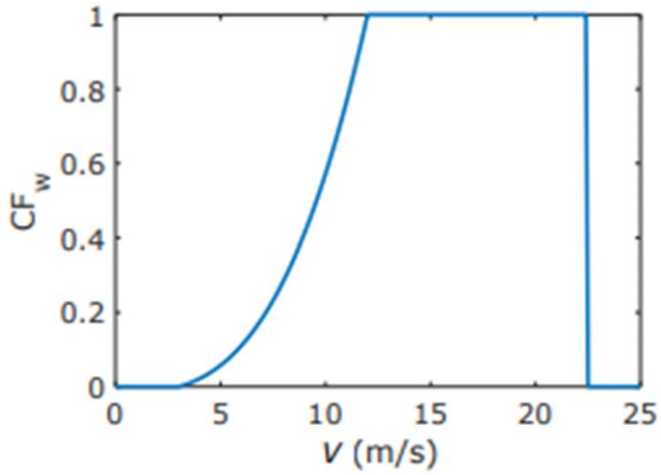

Figure 2 . Power curve for Vestas V126-3.3 wind turbine. Reproduced from [3] © IOP Publishing Ltd. CC BY 3.0.

After the modelling of the cell efficiency, the solar PV capacity factor (CF_S) is calculated by equation (3).

$$CF_s = \frac{\eta_{cell}(G,\ T)\ \cdot\ G}{\eta_{ref}\ \cdot\ G_{ref}} \tag{3}$$

where, a reference irradiation of $G_{ref} = 1000\ Wm^{-2}$ is considered as 'peak sun' [31]. It evident that the CF equation is independent of the reference cell efficiency and eventually cancels out since it appears in both the numerator and the denominator of equation (3). It is also important to note that influence from inverters are neglected in this modelling approach.

2.1.2.2. Wind capacity factors

The wind CF (CF_w) for a Vestas V126-3.3 wind turbine is modelled with the power curve equation as presented in equation (4) [3]. In this paper, we make the simplified assumption that this turbine is suitable for global coverage and various regional weather and climatic conditions. CF_w is calculated based on the turbine's hub height as:

$$CF_w = \begin{cases} 0, & for\ V \leqslant V_{in} \\ \dfrac{V^3 - {V_{in}}^3}{{V_r}^3 - {V_{in}}^3}, & for\ V_{in} < V \leqslant V_r \\ 1, & for\ V_r < V \leqslant V_c \\ 0, & for\ V > V_c \end{cases} \tag{4}$$

where $V_{in} = 3\ ms^{-1}$ is defined as the cut-in wind speed, $V_r = 12\ ms^{-1}$ is the rated wind speed and $V_c = 22.5\ ms^{-1}$ is the cut-off wind speed [32].

The Vestas V126-3.3 has a hub height of 117 m and rated power of 3.3 MW per turbine [32]. The power curve equation used in estimating CF_w is shown in figure 2.

For modelling of the wind power, we do not consider influence from low temperature shutoff [33].

2.1.3. Synergy metric

2.1.3.1. Normalised pearson correlation coefficient (monthly analysis)

The Pearson correlation coefficient is a widely used metric to quantify the seasonal complementarity between RE but in this study Pearson coefficient (equation (5)) has been normalised [10] to range from 0 to 1, where 0 refers to positive correlation between solar and wind, 0.5 denotes no correlation, and 1 denotes maximum synergy (negative correlation) between solar and wind power. Normalised Pearson correlation coefficient (r) is defined as follows:

Figure 3. Global map showing case study locations for solar PV and wind power synergy analysis. Black markers indicate location coordinates (see table S1 in supplementary information A for numerical coordinates).

$$r = 0.5\left[1 - \frac{cov(CF_s, CF_w)}{\sigma CF_s \sigma CF_w}\right] = \frac{1 - \frac{\sum_{year}(CF_s(t) - \overline{CF_s})(CF_w(t) - \overline{CF_w})}{\sqrt{\sum_{year}(CF_s(t) - \overline{CF_s})^2} \cdot \sqrt{\sum_{year}(CF_w(t) - \overline{CF_w})^2}}}{2} \quad (5)$$

Where CF_s, CF_w are given paired generation time series of solar and wind capacity factors, $\overline{CF}$ denotes a yearly average capacity factor, whereas cov and σ denotes covariance and standard deviation, respectively, and t is the time step (monthly).

2.1.3.2. Stability coefficient (hourly analysis)

The stability coefficient (C_{stab}) as developed by [3] is used to assess diurnal synergies between solar PV and wind power and is defined as:

$$C_{stab} = 1 - \frac{C_{v,mix}}{c_{v,s}} \quad (6)$$

$$C_{stab} = 1 - \frac{\sqrt{\sum_{day}(CF_{mix}(t) - \overline{CF}_{mix})^2}}{\sqrt{\sum_{day}(CF_s(t) - \overline{CF}_s)^2}} \times \frac{\overline{CF}_s}{\overline{CF}_{mix}} \quad (7)$$

$$CF_{mix} = \frac{nCF_s + mCF_w}{(n + m)} \quad (8)$$

where C_v is the coefficient of variation, subscripts s, w, mix denote solar, wind and hybrid mix, CF denotes capacity factor, t is the time step (sub-daily) and $\overline{CF}$ denotes a daily average capacity factor. The results of C_{stab} is interpreted as follows; $C_{stab} = 0$ indicates no synergy between RE and $C_{stab} = 1$ means that there is maximum synergy between RE (flat output profile of solar-wind combination). It important to note that the domain of $C_{stab} \leqslant 1$. As stated earlier, installed capacities of solar (n) and wind (m) is set to a 1:1 ratio in this study. This is reflected in the calculation of CF_{mix} (equation (8)). It is already important to note that the software allows users to choose any desired capacity ratio.

For the calculation of synergy metrics, geographical restrictions (60°S–60°N; 180°W–180°E) are applied to the exploitation of power from solar PV cells and wind turbines on a global scale. This then reduces the solar potential to areas considered available and suitable for electricity production. Even though the polar regions may be suitable for wind power exploitation, this restriction is done to make sure the matrix dimensions of wind and solar CF agree for estimation of the synergy metrics.

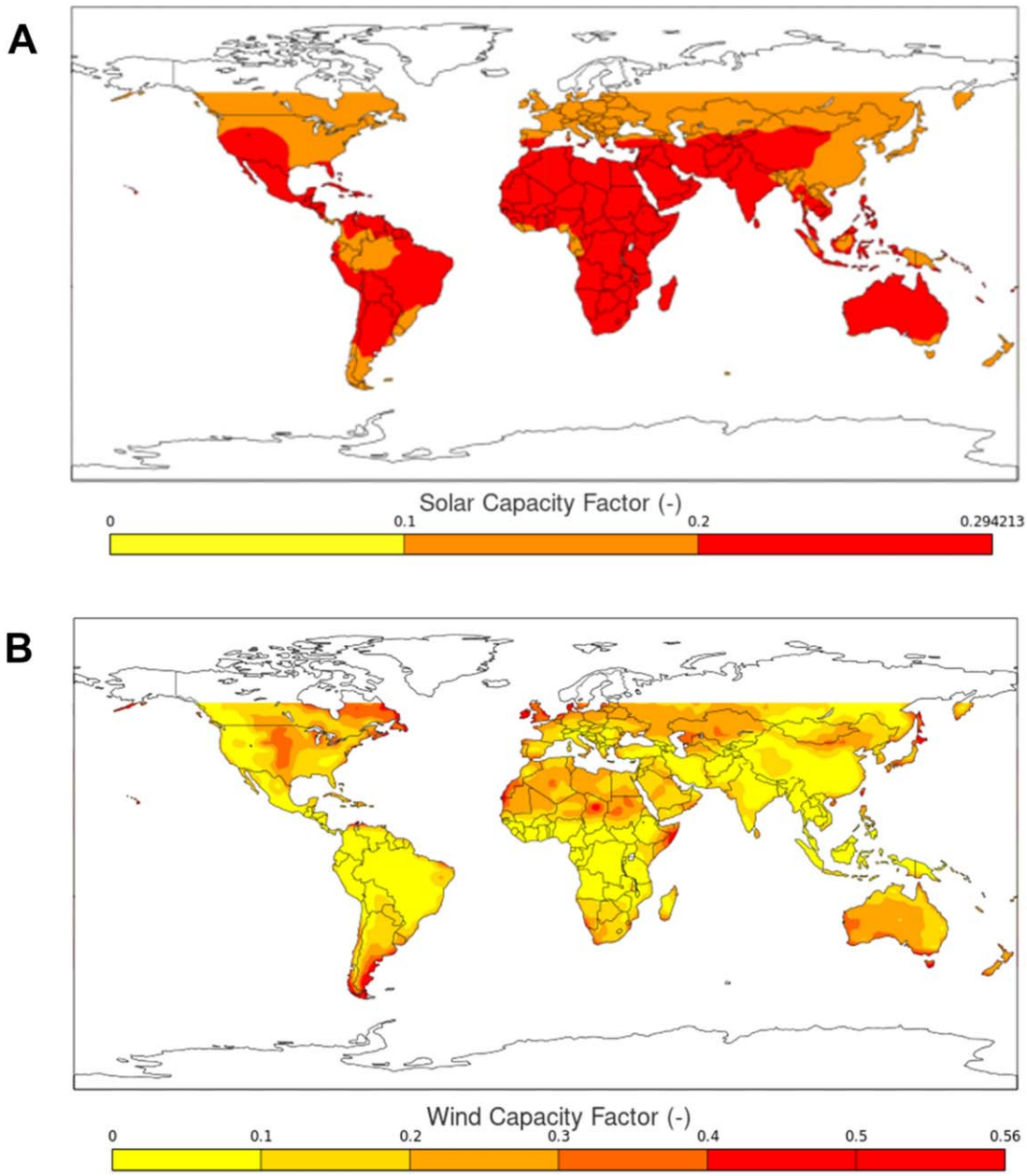

Figure 4. Global distribution of RE resource potential from 2011–2020 based on ERA5 data. (A) Annual average solar PV capacity factor; (B) Annual average wind capacity factor. Solar PV and wind CF are calculated based on monocrystalline silicon cells and Vestas V126-3.3 turbine respectively. Oceans and polar regions (above 60°N and below 60°S) are masked by white.

Table 1. Defined diurnal and seasonal synergy threshold.

Diurnal and Seasonal Synergy Threshold	
$C_{stab} > 0.4$	Good Diurnal Synergy
$0.2 < C_{stab} < 0.4$	Medium Diurnal Synergy
$C_{stab} < 0.2$	Bad Diurnal Synergy
$r > 0.7$	Good Seasonal Synergy
$0.5 < r < 0.7$	Medium Seasonal Synergy
$r < 0.5$	Bad Seasonal Synergy

2.2. Synergy performance for case study locations

Synergy performance across nine case study locations (figure 3) is studied. These case studies are selected arbitrarily with the aim of covering a wide range of types of solar-wind complementarity on the considered time scales.

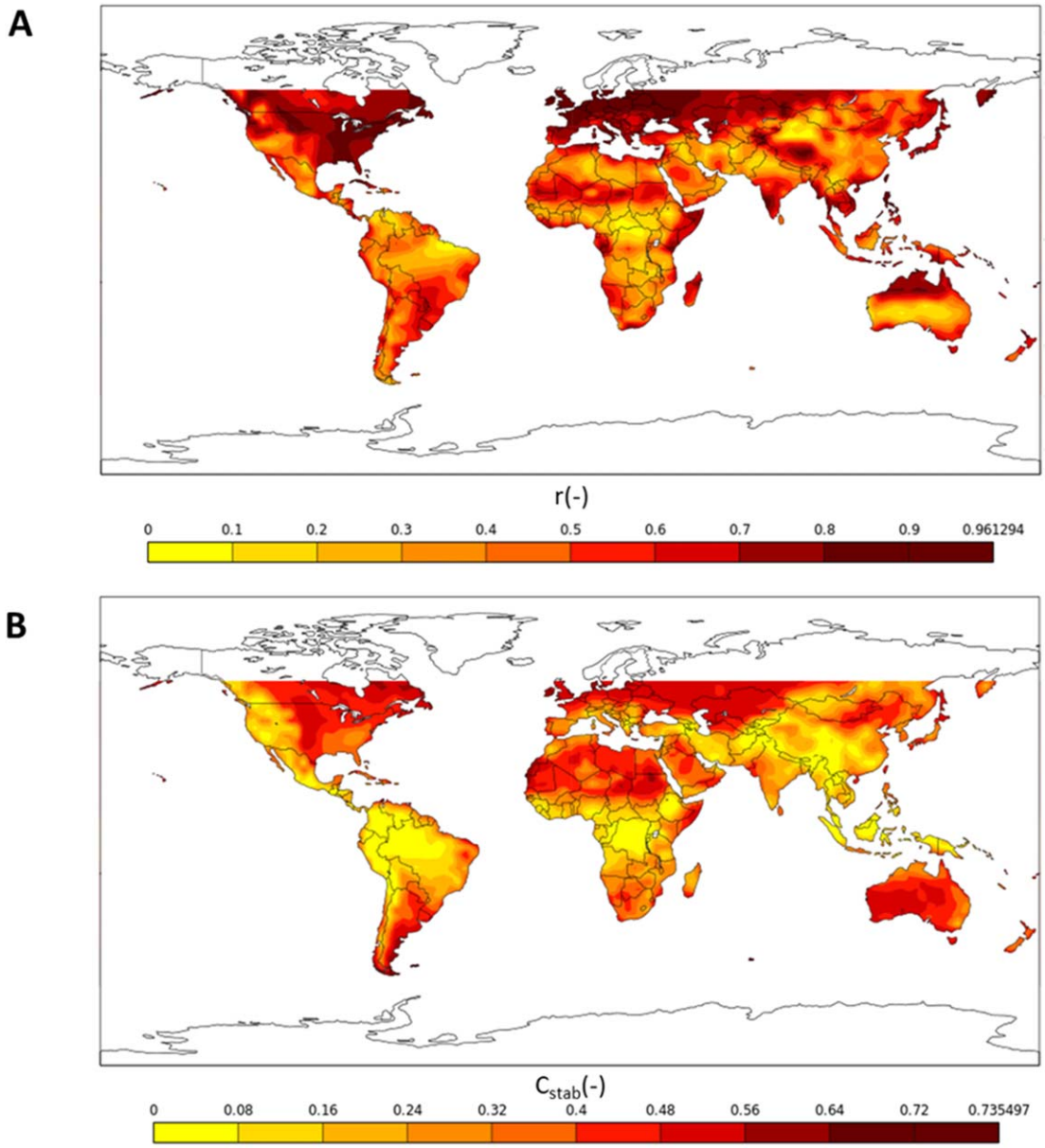

Figure 5. Global distribution of solar-wind synergy from 2011–2020. (A) Seasonal synergy: Annual average normalised Pearson coefficient (r). (B) Diurnal synergy: Annual average stability coefficient (C_{stab}). Oceans and polar regions (above 60°N and below 60°S) are masked by white.

Furthermore, characterization of case study locations into 'good', 'medium' and 'bad' diurnal and seasonal synergies based on pre-defined C_{stab} and r thresholds (table 1) is made. The selected thresholds are applied to the annually averaged diurnal and seasonal synergies for the respective locations. This categorization is subsequently extended to the entire globe including global analysis of 8 further variations of the selected threshold (see figures S11–S12 (available online at stacks.iop.org/ERC/4/055011/mmedia) in supplementary information A) and analyse the outcome. It is important to note here the selected threshold were chosen by the authors based on the seasonal and diurnal profiles observed across the case studies, and that different thresholds may lead to somewhat different results. In addition, we also categorise nonpolar regions with low solar or wind capacity factor (where CF $<$ 10% on an annual basis) as 'low resource areas'.

3. Results and discussion

3.1. Spatial distribution of average solar and wind potential

The average CF for monocrystalline silicon-based solar PV panels (figure 4(A)) highlights that the spatial variability of the solar PV potential is mainly driven by the distribution of global horizontal irradiation with minor dependence on temperature [2, 3, 29, 30]. Good solar CF can be found in regions such as Africa, the

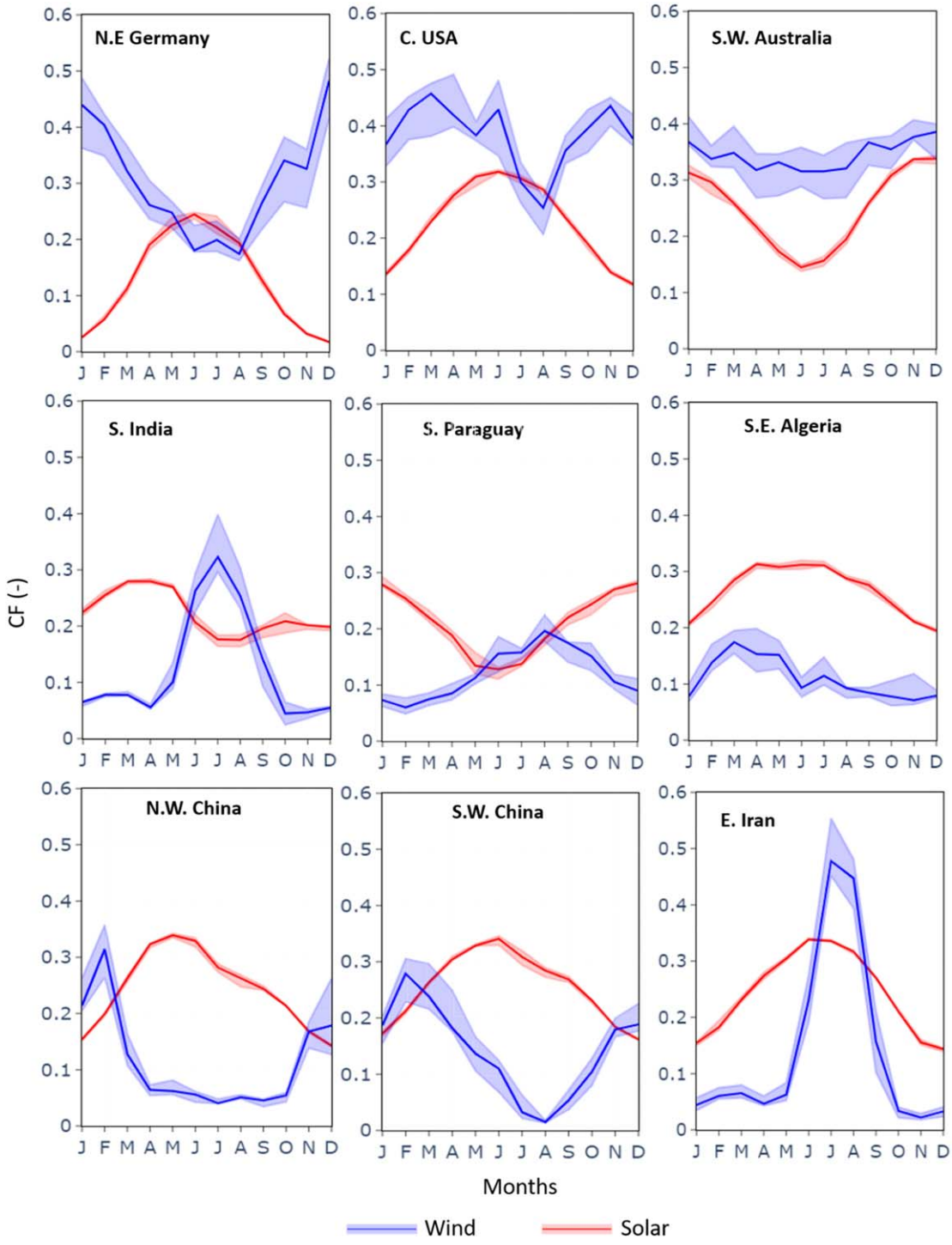

Figure 6. Seasonal solar PV and wind power profile from 2011–2020 for nine case study locations. Full lines represent median monthly capacity factors for solar PV (red) and wind (blue). Shaded uncertainty bands indicate the interquartile range.

Middle East, Northern Chile and its immediate neighbouring countries, Central and Northeastern Brazil, Australia, Mexico, Western China, and Western USA.

The spatial distribution of wind CF calculated for Vestas V126-3.3 turbines [32] (figure 4(B)) shows that high wind CF is mainly concentrated in the northern hemisphere and mid-to-high latitudes in the southern hemisphere where prevailing wind speeds are high. Low wind power potential is concentrated in the tropics with the minimum wind CF in the Amazon of South America and the Congo basin, corroborating earlier studies [34, 35].

Exploitation of RE in regions with high CF can be considered advantageous in terms of high electricity yield and favourable returns on investment. In practice, however, a major limitation such as capital investment and

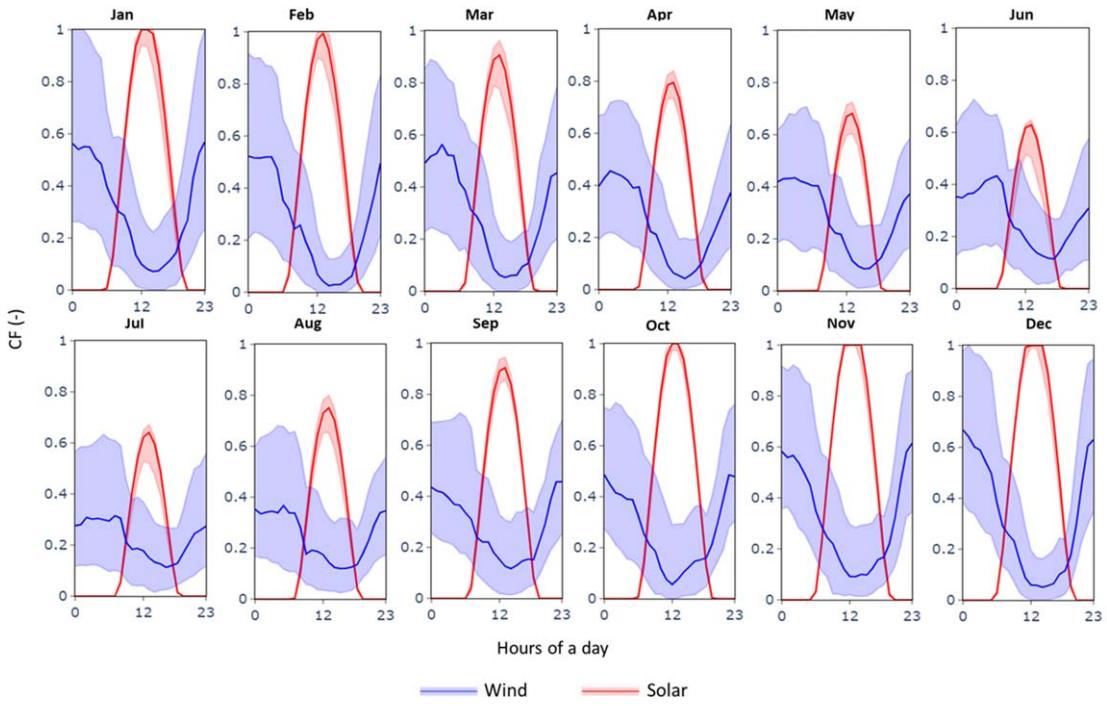

Figure 7. Diurnal solar and wind power profile by month from 2011–2020 for South West Australia. Full lines represent median monthly capacity factors for solar PV (red) and wind (blue). Shaded uncertainty bands indicate the interquartile range.

physical access to certain location within regions with high resource potential may hinder full exploitation of these resources.

3.2. Solar-wind synergies at the global scale

Next, we explore the seasonal complementary between solar PV and wind using the normalized Pearson correlation coefficient (figure 5(A)). In addition, considering a hybrid solar PV and wind power system with assumed equal installed capacity for both resources (capacity ratio of 1:1), we show the annual average complementarity between solar PV and wind on diurnal time scale using the stability coefficient (figure 5(B)).

On seasonal time scales, notable regions with high synergy ($r > 0.7$) are Europe, Southern India, Canada, USA (excluding the South Western USA), Western Russia, Kazakhstan, South Western China, and Northern Australia (figure 5(A)). Notable regions with poor seasonal synergies ($r < 0.5$) are Southern Australia, Northern India, North Western China, Pakistan, Afghanistan, and many regions in Sub-Saharan Africa (figure 5(A)). In the latter regions, solar PV potential is high (figure 4(A)) but typically subjected to a much less pronounced seasonality than wind power potential, lowering the scope for mutual complementarity.

On diurnal time scales, notable regions where high synergies ($C_{stab} > 0.4$) can be exploited are Central USA, Eastern Canada, Northern Europe, Western Russia, Central Asia, Australia, Southern Argentina and various regions of the Sahara and Sahel (figure 5(B)). Wind power potential is relatively strong over these regions and in some cases has a complementary diurnal cycle to solar PV, with winds blowing more strongly during night- than daytime. Regions with low wind power such as the Amazon in South America and Democratic Republic of the Congo show bad solar-wind complementarity ($C_{stab} < 0.2$) because wind power potential is too weak here to achieve substantial balancing effects.

Exploitation of RE for large-scale grid feed-in in regions of good seasonal and diurnal synergies will mean lower dependence on power storage. This will be beneficial in terms of costs resulting from storage deployment needs. Several of these regions could also explore other RE sources in addition to solar PV and wind, such as hydropower or biomass where available [12, 19, 36, 37].

3.3. Seasonal and hourly power profiles for case study locations

Northeast (N.E.) Germany shows the most pronounced complementarity ($r = 0.87 \pm 0.04$) between solar PV and wind on seasonal timescales compared to the other case study locations (figure 6; table 2). Even though locations such as Central (C.) USA and Southwest (S.W.) Australia would have comparable or even better annual average wind power yields (annual average wind CF of 37.9%(2.0pp) and 34.1%(1.0pp), respectively, as compared to 30.4%(2.0pp) for N.E. Germany; see table 2), solar-wind complementarity appears relatively less

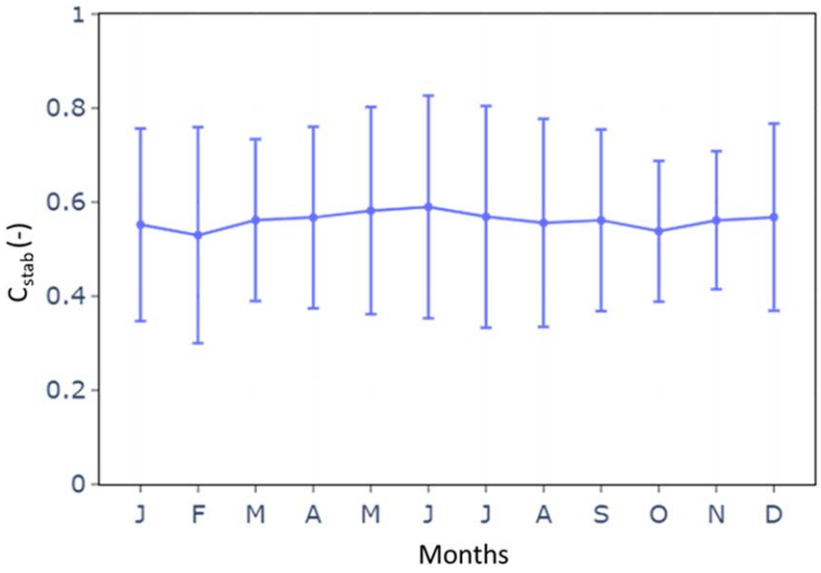

Figure 8. Monthly averaged stability coefficient from 2011–2020 for South West Australia. The error bars represent standard deviations across the study period.

Table 2. Annual averages of Solar CF, Wind CF, Normalised Pearson Correlation (r), and Stability Coefficient (C_{stab}) from 2011–2020. Case studies are ordered from high to low normalised pearson correlation. Standard deviation in parenthesis. pp = percentage points.

Region	Solar CF (%)	Wind CF (%)	r (—)	C_{stab} (—)
North East (N.E.) Germany	12.7 (0.5pp)	30.4 (2.0pp)	0.87 (0.04)	0.56 (0.02)
North West (N.W.) China	24.3 (0.4pp)	11.7 (1.0pp)	0.82 (0.06)	0.16 (0.01)
Southern (S.) India	22.1 (0.5pp)	12.7 (1.0pp)	0.73 (0.07)	0.32 (0.02)
South West (S.W.) China	25.4 (0.2pp)	14.6 (1.0pp)	0.69 (0.05)	0.17 (0.01)
Southern (S.) Paraguay	21.0 (0.7pp)	11.9 (0.9pp)	0.69 (0.13)	0.37 (0.01)
Central (C.) USA	22.5 (0.5pp)	37.9 (2.0pp)	0.59 (0.11)	0.55 (0.01)
South East (S.E.) Algeria	26.5 (0.3pp)	11.4 (0.8pp)	0.33 (0.13)	0.22 (0.02)
South West (S.W.) Australia	24.7 (0.4pp)	34.1 (1.0pp)	0.28 (0.11)	0.56 (0.01)
Eastern (E.) Iran	24.3 (0.2pp)	14.3 (2.0pp)	0.15 (0.02)	0.19 (0.02)

pronounced in those regions ($r = 0.59 \pm 0.11$ and 0.28 ± 0.11 respectively). In contrast, in locations such as Eastern (E.) Iran, solar and wind power do not have opposite seasonality and in fact peak in the same season (figure 6), implying low seasonal synergy ($r = 0.15 \pm 0.02$) [38, 39].

These results illustrate the clear impact of regional climate conditions on solar-wind synergies on seasonal timescales, such as temperate maritime climates with pronounced winter-summer differences like N.E. Germany, or monsoonal climates with rainy and dry seasons like Southern (S.) India. For instance, in S. India, strong southwest monsoon wind causes an increase in wind power during the monsoon season (June-September) with a decrease in solar power due to monsoon cloud cover (figure 6), leading to high seasonal synergies ($r = 0.73 \pm 0.07$) [40].

Considering an exemplary subtropical location such as S.W. Australia (figure 7), it is evident that on average, the diurnal cycle of wind power can make up for solar power deficits in the evenings and absence at night throughout the year for S.W. Australia. This is due to strong available nighttime wind resources in the southwestern part of Australia, balancing the strong daytime solar PV resource [41]. The diurnal profiles for the stated location shows particularly high synergies in the summer months (December to February), since these coincide with strong wind peaking at night, complementing solar PV (figure 7). Comparable solar-wind synergy is also noted in the winter (June to August) due to strong and less variable wind power, even though solar power is then relatively low (figure 7). Clearly, the seasonal profile of day-night synergies as quantified with the stability coefficient has very low variability on average (see figure 8): there is little seasonality in the diurnal synergies. On the other hand, the seasonal synergy between the two resources is relatively low (see table 2).

Strong day to night synergy of solar PV and wind power is also observed in temperate locations such as C. USA and N.E Germany, with the latter also showing a pronounced diurnal wind power cycle (see supplementary information A: figures S2 and S1 respectively) [42, 43]. On the contrary, even though S.W. China shows

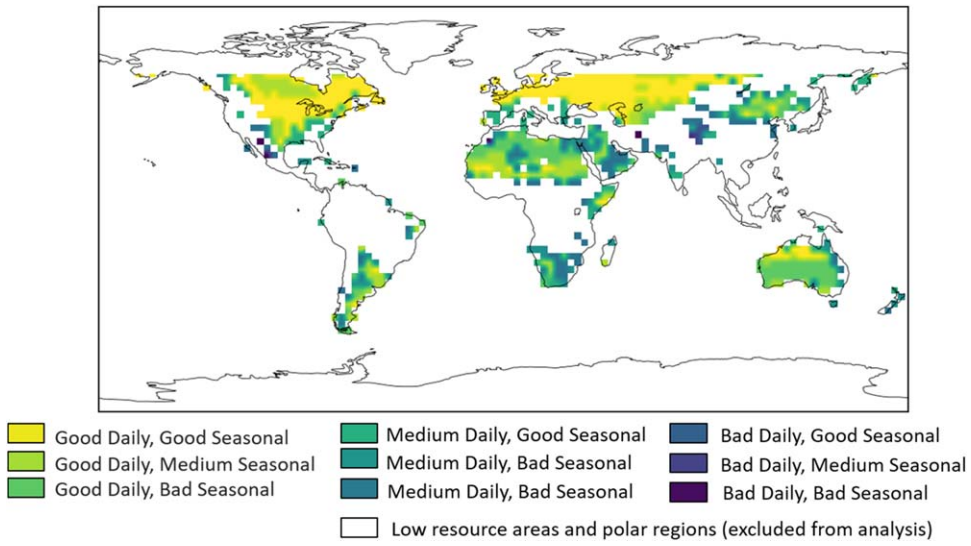

Figure 9. Global categorization of synergy performance for period 2011–2020. See table 1 for synergy metric threshold. Oceans and polar regions (above 60°N and below 60°S) are masked by white. Low resource area (also masked white) is defined as nonpolar regions with low solar or wind capacity factor (CF $<$ 10% on an annual basis).

Table 3. Categorization of synergy performance for 9 exemplary focal locations.

	Seasonal Synergy			
Diurnal Synergy		Good	Medium	Bad
	Good	N.E. Germany	C. USA	S.W. Australia
	Medium	S. India	S. Paraguay	S.E. Algeria
	Bad	N.W. China	S.W. China	E. Iran

pronounced diurnal wind cycles except in the summer months (June–September), wind and solar PV power have similar diurnal profiles, leading to low diurnal synergies (see supplementary information A: figure S7) [44].

The spatiotemporal distribution of the day-to-night solar and wind synergy is more strongly driven by the distribution of the wind resource than of the solar resource (see supplementary information A: figure S10). For instance, locations with weak wind resources (S. India, S. Paraguay, S.E Algeria [45], N.W. China and E. Iran) automatically reflect in low diurnal synergies (see figures S3–S6, S8 in supplementary information A). This is because the spatiotemporal variability of wind power potential, and the corresponding range of hourly CF values, is much more uneven across the globe than that of solar PV.

3.4. Categorizing synergy performance

Result from characterizing case study locations into 'good', 'medium' and 'bad' diurnal and seasonal synergies based on pre-defined C_{stab} and r thresholds (table 1) is shown in table 3. This categorization of synergy performance is subsequently extended to the entire globe (figure 9) with 8 further threshold variations (see supplementary information A: figures S11–S12). As stated earlier, categorization of case studies and regions is strictly dependent on the selected threshold and different thresholds may give somewhat different results.

Regions with both good diurnal and seasonal synergies include Northern Europe, Eastern Canada, Central USA, Western Russia, Kazakhstan, and Northern Australia (figure 9). Overall, 14% of all land area is covered by this category (see figure 10 and quadrant C in figure 11). Central Canada, most of Northern Africa, few regions in Central Asia, Eastern Argentina, and North-eastern China are notable regions with good diurnal and medium seasonal synergies (see figure 9). The fraction of land area covered by this category is 10% (see figure 10 and quadrant B in figure 11). Most of the remaining regions are concentrated in the good diurnal and bad seasonal synergy zone, land area fraction of 10% (figure 10 and quadrant A in figure 11). While a few regions show medium diurnal with bad, medium and good seasonal synergies, (see figures 9 and 10 and quadrant D–F in figure 11), there are little to no regions in the bad diurnal with bad, medium, and good seasonal synergy zones (see figure 10 and quadrant G–I in figure 11).

Simultaneous occurrence of bad daily and seasonal synergies would mean that even though solar and wind resources would be available, synergy would be bad due to poor complementing profiles. Our results show that such regions are extremely rare globally (0.32% of global land area, see figure 10 and quadrant G in figure 11), a

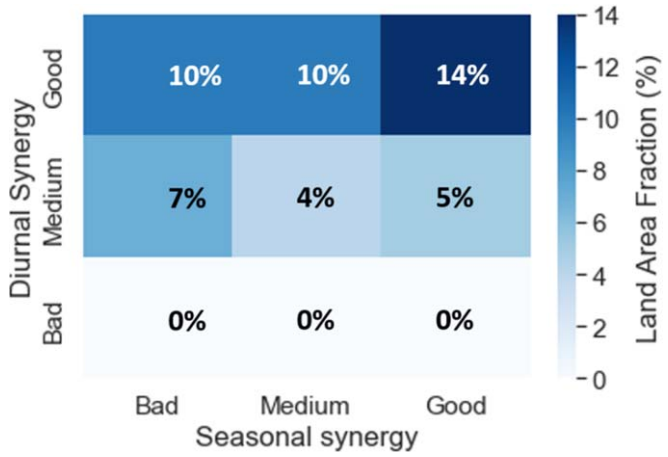

Figure 10. Heatmap of fraction of non-polar land area (%) covered by each synergy category for period 2011–2020. Percentages are rounded to integers. Fraction of low resource area within the non-polar land area is 49%.

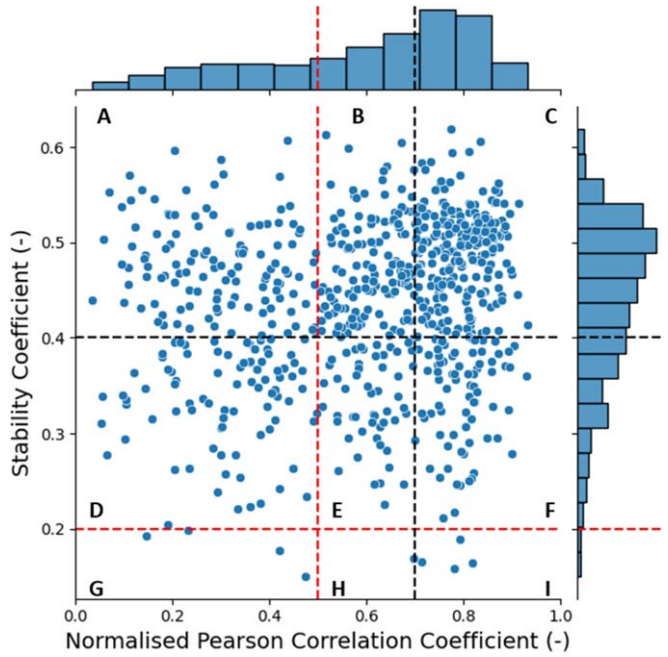

Figure 11. Marginal plot distribution of stability coefficient (—) and normalised Pearson correlation coefficient (—). Red dash (black dash) are threshold for bad (good) diurnal and seasonal synergies based on of stability coefficient and normalised Pearson correlation coefficient respectively (see table 1). Quadrant A indicates all grid cells with good diurnal but bad seasonal synergies; B indicates all grid cells with good diurnal but medium seasonal synergies; C indicates all grid cells with good diurnal and seasonal synergies; D indicates all grid cells with medium diurnal but bad seasonal synergies; E indicates all grid cells with medium diurnal and seasonal synergies; F indicates all grid cells with medium diurnal but good seasonal synergies; G indicates all grid cells with bad diurnal and seasonal synergies; H indicates all grid cells with bad diurnal but medium seasonal synergies; I indicates all grid cells with bad diurnal and good seasonal synergies.

result which is largely insensitive to the choice of threshold values for C_{stab} and r (see supplementary information A: figures S11–S12). Thus, medium-to-good seasonal and diurnal complementarity between solar and wind is the rule, rather than the exception, in regions with exploitable resources.

3.5. Limitations

Our analysis has important uncertainties and limitations. This study only focuses on the geographical limit of exploring synergic benefits of solar and wind on land without any consideration of economic feasibility. In addition, the use of simplified modelling approach of solar PV capacity factor (without consideration of inverters), generalization of the wind turbine technology (without considerations of low temperature shut-off) and spatial resolution for analysis may have significant effect on the distribution of solar and wind capacity

factors respectively. The study also focuses only on the supply side of synergy analysis and assumes equal installed capacity of hybrid solar and wind system, which may affect the distribution of synergies. Finally, selected threshold specifically for the categorisation of regions into good, medium and bad synergies are arbitrary and different threshold may have significant effect on the categorized distribution (especially regions in the medium to good diurnal and seasonal synergic zones) (figure 9). Despite this simplifying assumption, results from this study may be of importance for exploratory solar-wind synergic assessment before any detailed analysis for a region or location is performed.

4. Conclusion

In this study, solar-wind synergies on seasonal and diurnal timescale across the globe have been investigated across several range of assumptions using the normalized Pearson correlation coefficient (r) and the stability coefficient (C_{stab}), respectively.

We analysed synergy patterns across nine case study locations including all types of daily and seasonal synergy going from good to poor synergies. Finally, we demonstrated that in regions with reasonable resources, complementarity between solar and wind is the norm rather than the exception. Even though categorisation of regions is dependent on the power generation technology and choice of threshold for synergy metrics, they are unlikely to change the overall prior conclusion of this study.

Effective exploitation of synergic power depends on local and regional demand profiles and a readily available electricity grid. This study focuses on supply-side synergies: while considering demand profiles would be beneficial for further exploring potential synergies or trade-offs, we believe it would engender large uncertainty due to data availability challenges at regional to global scales. Also, regions may need to expand existing grid and construct new power grids to unlock the hybrid solar PV-wind complementarity. Local and regional power grid presence and expansion is beyond the scope of this study and hence not considered.

This study is only a first step in evaluating more in-depth the synergetic roles that solar and wind power could play in tandem on worldwide scales in future power systems—with important aspects such as complementarity with demand profiles falling outside of the scope of this study. Yet, an important lesson that could be retained from this analysis is the fact that the contributions of solar and wind power should perhaps, in many regions of the world planning for an energy transition, be considered as a unit from the outset. Instead of developing, for instance, separate assessments of national solar power potential or wind power potential, all considerations related to these forms of variable renewable electricity generation could be done right from the start with their potential synergies in mind. This can aid in the designing of robust hybrid energy systems and diminish fears of diurnal or seasonal imbalances in the power mix.

Also, this study may contribute to determining smart mixes of RE resources for power systems planning, when combined with local and regional environmental and socioeconomic policies.

An open-source software, **R**enewable **El**ectric**it**y Syn**e**rgy (*RELITE*), used to run the analysis and generate the results provided in this paper, is hosted on European Copernicus cloud and is publicly available via the link (https://cds.climate.copernicus.eu/toolbox-editor/50153/relite). With RELITE local, regional and global synergy analysis can be performed considering different wind turbine technologies with defined cut-in, nominal and cut-out wind speeds. Currently RELITE is limited to monocrystalline silicon-based solar PV cells for synergy analysis. This limitation may be improved in future RELITE versions. The software manual can be found in the supplementary information B. A free user account is required to access the software.

Acknowledgments

S S and W T acknowledge research funding from the project CIREG (Climate Information for Integrated Renewable Electricity Generation), which is part of ERA4CS, an ERA-NET Co-fund action initiated by JPI Climate, funded by BMBF (Germany), FORMAS (Sweden), BELSPO (Belgium) and IFD (Denmark) with co-funding from the European Union's Horizon2020 Framework Program (Grant 690462).

Data availability statement

All data that support the findings of this study are are available at (https://cds.climate.copernicus.eu/toolbox-editor/50153/relite). Supplementary files are included within the article.

Code availability

The code used to generate the paper's results are available at (https://cds.climate.copernicus.eu/toolbox-editor/50153/relite).

Author contributions

E N, S S and W T designed the study. E N performed the analysis and wrote the manuscript. All authors reviewed the manuscript.

ORCID iDs

Emmanuel Nyenah https://orcid.org/0000-0001-8766-7657
Sebastian Sterl https://orcid.org/0000-0003-1078-5561

References

[1] Aberg E *et al* 2019 Climate change and renewable energy national policies and the role of communities, cities and regions: A report from the International Renewable Energy Agency (IRENA) to the G20 Climate Sustainability Working Group (CSWG), (https://irena.org/-/media/Files/IRENA/Agency/Publication/2019/Jun/IRENA_G20_climate_sustainability_2019.pdf)
[2] Chen S, Lu X, Miao Y, Deng Y, Nielsen C P, Elbot N, Wang Y, Logan K G, McElroy M B and Hao J 2019 The potential of photovoltaics to power the belt and road initiative *Joule* **3** 1895–912
[3] Sterl S, Liersch S, Koch H, van Lipzig N P M and Thiery W 2018 A new approach for assessing synergies of solar and wind power: implications for West Africa *Environmental Research Letters* **13** 094009
[4] Jurasz J, Canales F A, Kies A, Guezgouz M and Beluco A 2020 A review on the complementarity of renewable energy sources: concept, metrics, application and future research directions *Solar Energy* **195** 703–24
[5] Tong D, Farnham D J, Duan L, Zhang Q, Lewis N S, Caldeira K and Davis S J 2021 Geophysical constraints on the reliability of solar and wind power worldwide *Nature Communications* **12** 6146
[6] Gielen D, Boshell F, Saygin D, Bazilian M D, Wagner N and Gorini R 2019 The role of renewable energy in the global energy transformation *Energy Strategy Reviews* **24** 38–50
[7] International Renewable Energy Agency (IRENA) 2021 Renewable Capacity Statistics 2021, (https://irena.org/-/media/Files/IRENA/Agency/Publication/2021/Apr/IRENA_RE_Capacity_Statistics_2021.pdf)
[8] Shaner M R, Davis S J, Lewis N S and Caldeira K 2018 Geophysical constraints on the reliability of solar and wind power in the United States *Energy and Environmental Science* **11** 914–25
[9] Drechsler M, Egerer J, Lange M, Masurowski F, Meyerhoff J and Oehlmann M 2017 Efficient and equitable spatial allocation of renewable power plants at the country scale *Nature Energy* **2**
[10] Zhang H, Cao Y, Zhang Y and Terzija V 2018 Quantitative synergy assessment of regional wind-solar energy resources based on MERRA reanalysis data *Applied Energy* **216** 172–82
[11] Takle E S and Shaw R H 1979 Complimentary nature of wind and solar energy at a continental mid-latitude station *International Journal of Energy Research* **3** 103–12
[12] Sterl S, Fadly D, Liersch S, Koch H and Thiery W 2021 Linking solar and wind power in eastern Africa with operation of the grand ethiopian renaissance dam *Nature Energy* **6** 407–18
[13] Sterl S, Vanderkelen I, Chawanda C J, Russo D, Brecha R J, van Griensven A, van Lipzig N P M and Thiery W 2020 Smart renewable electricity portfolios in West Africa *Nature Sustainability* **3** 710–9
[14] François B, Borga M, Creutin J D, Hingray B, Raynaud D and Sauterleute J F 2016 Complementarity between solar and hydro power: sensitivity study to climate characteristics in Northern-Italy *Renewable Energy* **86** 543–53
[15] Becker S, Frew B A, Andresen G B, Zeyer T, Schramm S, Greiner M and Jacobson M Z 2014 Features of a fully renewable US electricity system: optimized mixes of wind and solar PV and transmission grid extensions *Energy* **72** 443–58
[16] Miglietta M M, Huld T and Monforti-Ferrario F 2016 Local complementarity of wind and solar energy resources over europe: an assessment study from a meteorological perspective *Journal of Applied Meteorology and Climatology* **56** 217–34
[17] Heide D, von Bremen L, Greiner M, Hoffmann C, Speckmann M and Bofinger S 2010 Seasonal optimal mix of wind and solar power in a future, highly renewable Europe *Renewable Energy* **35** 2483–9
[18] Hoicka C E and Rowlands I H 2011 Solar and wind resource complementarity: advancing options for renewable electricity integration in Ontario, Canada *Renewable Energy* **36** 97–107
[19] Sterl S, Donk P, Willems P and Thiery W 2020 Turbines of the Caribbean: decarbonising Suriname's electricity mix through hydro-supported integration of wind power *Renewable & Sustainable Energy Reviews* **134** 110352
[20] Canales F A, Jurasz J, Beluco A and Kies A 2020 Assessing temporal complementarity between three variable energy sources through correlation and compromise programming *Energy* **192**
[21] Jurasz J, Mikulik J, Dąbek P B, Guezgouz M and Kaźmierczak B 2021 Complementarity and 'resource droughts' of solar and wind energy in Poland: an ERA5-based analysis *Energies* **14** 1118
[22] Canales F A, Jurasz J, Kies A, Beluco A, Arrieta-Castro M and Peralta-Cayón A 2020 Spatial representation of temporal complementarity between three variable energy sources using correlation coefficients and compromise programming *MethodsX* **7** 100871
[23] Raoult B, Bergeron C, López Alós A, Thépaut J-N and Dee D 2017 Climate service develops user-friendly data store, (https://ecmwf.int/sites/default/files/elibrary/2017/18188-climate-service-develops-user-friendly-data-store.pdf)
[24] Nefabas K L, Söder L, Mamo M and Olauson J 2021 Modeling of ethiopian wind power production using era5 reanalysis data *Energies* **14**
[25] Olauson J 2018 ERA5: the new champion of wind power modelling? *Renewable Energy* **126** 322–31

[26] Urraca R, Huld T, Gracia-Amillo A, Martinez-de-Pison F J, Kaspar F and Sanz-Garcia A 2018 Evaluation of global horizontal irradiance estimates from ERA5 and COSMO-REA6 reanalyses using ground and satellite-based data *Solar Energy* **164** 339–54
[27] Dee D P *et al* 2011 The ERA-Interim reanalysis: configuration and performance of the data assimilation system *Quarterly Journal of the Royal Meteorological Society* **137** 553–97
[28] Hersbach H *et al* 2020 The ERA5 global reanalysis *Quarterly Journal of the Royal Meteorological Society* **146** 1999–2049
[29] Crook J A, Jones L A, Forster P M and Crook R 2011 Climate change impacts on future photovoltaic and concentrated solar power energy output *Energy and Environmental Science* **4** 3101–9
[30] Wild M, Folini D, Henschel F, Fischer N and Müller B 2015 Projections of long-term changes in solar radiation based on CMIP5 climate models and their influence on energy yields of photovoltaic systems *Solar Energy* **116** 12–24
[31] Park S H, Roy A, Beaupré S, Cho S, Coates N, Moon J S, Moses D, Leclerc M, Lee K and Heeger A J 2009 Bulk heterojunction solar cells with internal quantum efficiency approaching 100% *Nature Photonics* **3** 297–302
[32] Vestas 2021 Vestas V126-3.3, *Wind-Turbine-Models.com*
[33] Wallenius T and Lehtomäki V 2016 Overview of cold climate wind energy: challenges, solutions, and future needs *Wiley Interdisciplinary Reviews: Energy and Environment* **5** 128–35
[34] Lu X, McElroy M B and Kiviluoma J 2009 Global potential for wind-generated electricity *Proceedings of the National Academy of Sciences of the United States of America* **106** 10933–8
[35] Archer C L and Jacobson M Z 2005 Evaluation of global wind power *Journal of Geophysical Research D: Atmospheres* **110** 1–20
[36] Gernaat D E H J, de Boer H S, Daioglou V, Yalew S G, Müller C and van Vuuren D P 2021 Climate change impacts on renewable energy supply *Nature Climate Change* **11** 119–25
[37] Srinivas T and Reddy B V 2014 Hybrid solar–biomass power plant without energy storage *Case Studies in Thermal Engineering* **2** 75–81
[38] Mostafaeipour A, Sedaghat A, Dehghan-Niri A A and Kalantar V 2011 Wind energy feasibility study for city of Shahrbabak in Iran *Renewable and Sustainable Energy Reviews* **15** 2545–56
[39] Gorjian S, Zadeh B N, Eltrop L, Shamshiri R R and Amanlou Y 2019 Solar photovoltaic power generation in Iran: Development, policies, and barriers *Renewable and Sustainable Energy Reviews* **106** 110–23
[40] Dunning C M, Turner A G and Brayshaw D J 2015 The impact of monsoon intraseasonal variability on renewable power generation in India *Environmental Research Letters* **10**
[41] Prasad A A, Taylor R A and Kay M 2017 Assessment of solar and wind resource synergy in Australia *Applied Energy* **190** 354–67
[42] Drücke J, Borsche M, James P, Kaspar F, Pfeifroth U, Ahrens B and Trentmann J 2021 Climatological analysis of solar and wind energy in Germany using the Grosswetterlagen classification *Renewable Energy* **164** 1254–66
[43] Camargo L R, Gruber K, Nitsch F and Dorner W 2019 Hybrid renewable energy systems to supply electricity self-sufficient residential buildings in Central Europe *Energy Procedia* **158** 321–6
[44] Ren G, Wan J, Liu J and Yu D 2019 Spatial and temporal assessments of complementarity for renewable energy resources in China *Energy* **177** 262–75
[45] Guezgouz M, Jurasz J, Chouai M, Bloomfield H and Bekkouche B 2021 Assessment of solar and wind energy complementarity in Algeria *Energy Conversion and Management* **238** 114170